Robotica (2011) volume 29, pp. 717–731. © Cambridge University Press 2010
doi:10.1017/S0263574710000627

Sagittal stability PD controllers for a biped robot using a neurofuzzy network and an SVR

João P. Ferreira†,‡*, Manuel Crisóstomo‡ and A. Paulo Coimbra‡

†*Department of Electrical Engineering, Superior Institute of Engineering of Coimbra, Rua Pedro Nunes-Quinta da Nora, Coimbra 3030-199, Portugal*
‡*Department of Electrical and Computer Engineering, Institute of Systems and Robotics, University of Coimbra, Polo 2-Pinhal de Marrocos, Coimbra 3030-290, Portugal. E-mail: mcris@isr.uc.pt, acoimbra@deec.uc.pt*

(Received in Final Form: September 15, 2010. First published online: October 12, 2010)

SUMMARY

The real-time balance PD control of an eight-link biped robot using a zero-moment point (ZMP) dynamic model is implemented using two alternative intelligent computing control techniques that were compared: one based on support vector regression (SVR) and another based on a first order Takagi–Sugeno–Kang (TSK) -type neural-fuzzy (NF). Both methods use the ZMP error, and its variation as inputs and the output is the correction of the robot's torso necessary for its sagittal balance. The SVR and the NF were trained based on simulation data, and their performance was verified with a real biped robot. Two performance indexes are proposed to evaluate and compare the online performance of the two control methods.

The ZMP is calculated by reading four force sensors placed under each robot's foot. The gait implemented in this biped is based on ankle and hip human trajectories that were acquired and adapted to the robot's size. Some experiments are presented and the results show that the implemented gait combined either with the SVR controller or with the TSK NF network controller can be used to control this biped robot. The SVR and the NF controllers exhibit similar stability, but the SVR controller runs at 0.2 ms, about 50 times faster than the NF controller and much faster than a controller based on full ZMP dynamic model equations.

KEYWORDS: Neural-fuzzy (NF) networks; Support vector regression (SVR); Biped robot; Balance; Zero-moment point (ZMP).

1. Introduction

Quite a number of biped humanoid robots have been developed, such as ASIMO by Honda,[1] WABIAN 2R by Waseda University,[2] HUBO KHR-3 by KAIST[3] and QRIO by Sony.[4] A biped robot's leg has a structure similar to human anatomy. To remain stable under dynamic situations such a robotic system requires good mechanical design, force sensors to acquire the zero-noment point (ZMP) and the design of appropriate real-time controllers.

Vukobratović *et al.* have developed a mathematical model of a biped robot and its method of control.[5] Other researchers have proposed dynamic biped models and methods of biped robot control.[12,21,33,35–38] Many researchers[6–8] have investigated the gait of biped robots based on human kinematics data, and Winter[9] has published a very good study of the kinematics of a human body. Because a biped robot is easily knocked down, to assure its dynamic stability, Hirai *et al.* proposed a standard method for gait synthesis based on the ZMP.[10] Basically, this method consists of designing a desired ZMP trajectory with online control corrections being made to the movement of the torso and pendulum afterward, during the robot's motion, based on the measurements from the feet's force sensors to achieve the defined ZMP trajectory.

Intelligent computing techniques have been widely used in the advanced control of biped robots, due to their strong learning and cognitive abilities and good tolerance of uncertainty and imprecision. Many researchers have been trying to solve the biped robot's balance problem by developing controllers, using intelligent computing methods such as fuzzy, neural networks, or neural-fuzzy (NF) networks,[16–21] support vector regression (SVR),[25] genetic algorithms,[39,40] and wavelet networks.[41,42] A survey of these techniques has been undertaken by Katic and Vukobratović[22] Park *et al.*[23] presented experimental results on ZMP compensation in the standing posture of a biped robot. They applied an external force in the sagittal plane to the biped robot and developed a ZMP compensation scheme using two-mode Q-learning. Recently, hybrid methods, using different computational intelligent techniques like reinforcement learning (RL) with simplified dynamics, have attracted attention for robot movement planning and control.[31–35] Each of these paradigms has its own merits and drawbacks. RL is a kind of learning algorithm half-way between supervised and unsupervised learning algorithms. The RL concept is based on trial and error methodology and continuous evaluation of performance in constant interaction with the environment.

Controlling a biped robot using the ZMP with an eight-link model is more accurate than the methods based on a two-link model with mass concentrations that are normally used for their real-time balance control. These methods use a two-link model centered in the ankle[12–14] or in the hip[15] to determine and apply the necessary torque for the robot's balance. In a recent past, it has been difficult to apply sagittal balance control in real time using an eight-link model of the

* Corresponding author. E-mail: ferreira@isec.pt

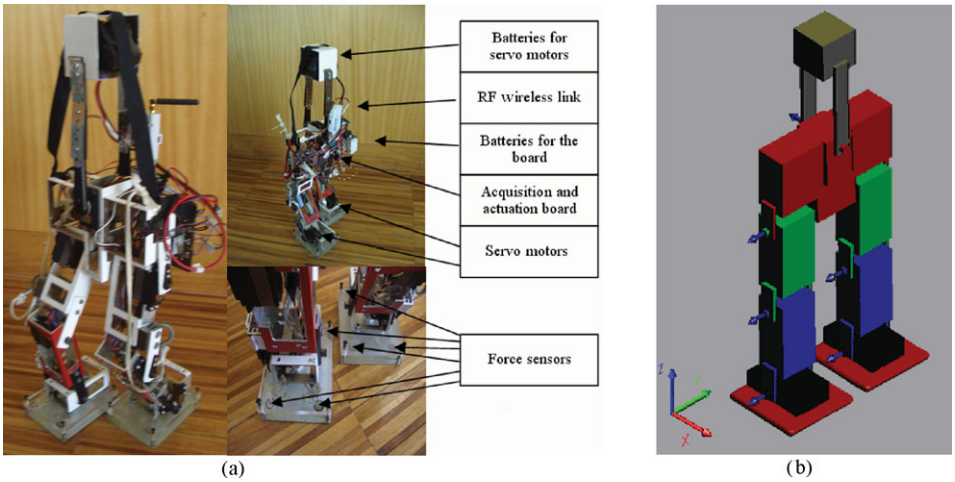

Fig. 1. (a) Implemented robot and (b) simplified robot model with global coordinate system axes and rotation axis of each joint.

robot due to the high computational effort. This problem is also reported by Or and Takanishi in ref. [43], where they say that the recent developments in the Sony QRIO and Honda ASIMO robots allow them to dance without falling, but their movements are prerecorded because the ZMP algorithms, which allow them to walk stably, are too computationally intensive to be applied in real time.

The present work solves this problem by using computational intelligence techniques (SVR and NF). The SVR and the NF are trained with the simulation data of an eight-link robot model and data generated by empirical rules based on the Ziegler–Nichols method.[30] As the ZMP control is nonlinear, an SVR is appropriate because it calculates the optimal hyper plane for data training and is faster than a neural network. The SVR technique was initially developed by Vapnik.[24] Another technique that is appropriate for this kind of problem is a first-order Takagi–Sugeno–Kang (TSK) type NF network. This technique offers the advantages of both fuzzy systems and neural networks. Using the eight-link biped model together with one of these two computational intelligence techniques, it is possible to control the biped robot in real time with greater precision than if the biped robot's simplified two-link model were used. These two proposed balance control methods have been compared and the results show that the gait used combined with the SVR controller or TSK NF network controller are appropriate for use in the control of this biped robot. Two performance indexes are also proposed to evaluate and compare the online performance of the biped robot's control methods. Using the proposed performance indexes, it is possible to conclude that the performance of the SVR and of the NF controllers is similar, although the SVR controller is much faster.

The gait implemented in this biped robot is based on ankle and hip human trajectories. A human gait was acquired and adapted to the size of the robot used. A feedforward (FF) backpropagation neural network was then trained to generate the robot's joint trajectories.

2. Implemented Robot

The experiments were performed with a biped robot that was designed and built at the Institute of System and Robotics of the Department of Electrical and Computer Engineering of the University of Coimbra, Portugal. The mechanical structure of the robot, as shown in Fig. 1(a), has the main joints of hip, knee, and ankle, for each leg, with 1-degree of freedom (DOF) for each joint, as shown in Fig. 1(b). This configuration was chosen because of its simplicity, the lateral balance being performed with only one joint. The other joints are used for the sagittal movement and balance control. There is another joint, an active inverted pendulum that is used for the lateral balance of the structure. The robot carries its own motorization batteries at this inverted pendulum. The robot is driven by seven servo motors, its structure is aluminum and acrylic, it weighs 2.3 kg, and it is 0.5 m tall. The robot was designed to move in both horizontal and inclined planes, to go up and down stairs (about 3 cm in height), and it moves at approximately 0.05 m/s. A 9600 bit/s RS232 wireless transmission link connects the control software, which is running on a PC, to the robot's electronic board. The robot board has two programmable interface controller (PIC) microprocessors, one to acquire the analog signals of the force sensors and the other to control the servo motors. The robot has a set of four force sensors under each foot, which are used to calculate the real ZMP, enabling the use of a closed-loop controller.

3. Designed Gaits

One of the best biped walkers is the human being. This is why the joint trajectories of a human walk were obtained and similar trajectories applied to this biped robot.[45] A gait was chosen for this work that was conceived to be similar to human locomotion in horizontal planes. Only the hip and ankle trajectories are needed to describe a robotic human-like gait. The knee trajectory depends on these two trajectories. The sagittal plane trajectories of hip, knee, ankle, and torso during a gait cycle of a person were acquired. The acquisition system used captures a sequence of images and determines the trajectories of five reference points.[8] Images were captured with a color webcam that had the following characteristics: CMOS 640 × 480 (VGA) sensor, maximum of 30 frames/s, USB 2 interface. Trajectory data were obtained with a 26-year-old male, 1.85-m tall. Light

https://doi.org/10.1017/S0263574710000627 Published online by Cambridge University Press

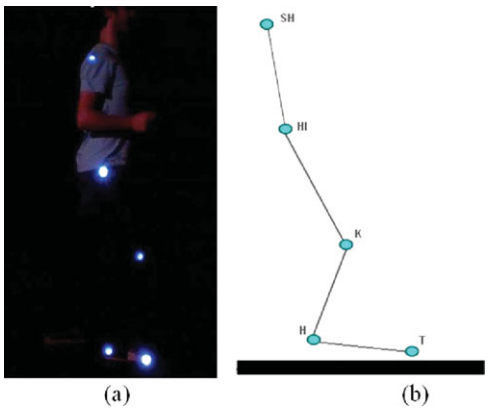

Fig. 2. (a) White light LED used as reference points on the person and (b) reference points on the person's model.

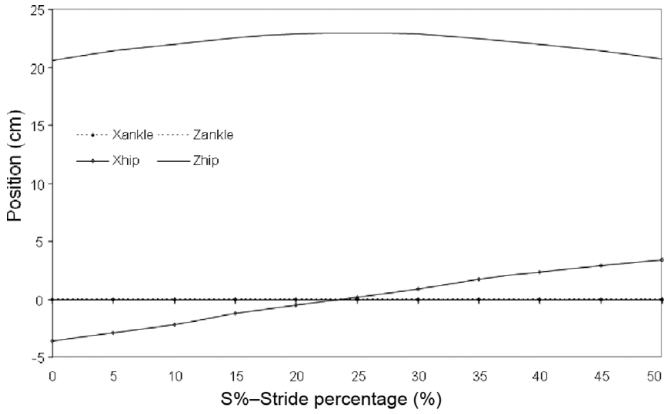

Fig. 3. Hip and ankle trajectories of the grounded foot (X_{ankle} and Z_{ankle} are zero).

emitting diodes (LED) were placed on five strategic points on him [see Fig. 2(a)], chosen to acquire the ankle, knee, hip, and torso sagittal trajectories according to the model in Fig. 2(b), where H is a point on the heel, T is the tip of the foot, K is a point on the knee, HI is a point on the hip, and SH is a point on the shoulder.[45] These reference points were captured by placing the camera perpendicular to the background plane, 3 m away from it and 0.75 m from the floor. This latter distance is half the distance from the floor to the highest reference point, which is the shoulder mark. After the image acquisition of the reference marks areas, the coordinates of the mass centers of these reference areas were calculated, in order to determine the trajectories of these points.

3.1. Normalized human gait trajectories

The trajectories acquired were normalized to be able to apply them to any robot, using the height of the leg (Z_{L}) and the step length (X_{S}) as scale factors. A set of polynomial regressions was then applied to the trajectories of the hip and the ankle resulting in the matrix expressions (1) and (2). The *R*-square obtained in these regressions was greater than 0.996, and the degrees of the polynomials are between 1 and 5. The polynomials described by (1) correspond to the trajectories during the first half of the gait cycle, when the foot is grounded, and the polynomials described by (2) correspond to the second half of the gait cycle, when the foot is moving.

$$\begin{bmatrix} X_{\text{hip}} \\ Z_{\text{hip}} \\ X_{\text{ankle}} \\ Z_{\text{ankle}} \end{bmatrix}^{T}_{\text{gnd}} = (AG_{\text{gnd}})^{T} XZ_{\text{gnd}}, \tag{1}$$

$$\begin{bmatrix} X_{\text{hip}} \\ Z_{\text{hip}} \\ X_{\text{ankle}} \\ Z_{\text{ankle}} \end{bmatrix}^{T}_{\text{mov}} = (AG_{\text{mov}})^{T} XZ_{\text{mov}}. \tag{2}$$

A is a polynomial coefficient matrix, G_{gnd} is the percentage of the gait cycle vector for the grounded foot, G_{mov} is the percentage of the gait cycle vector for the moving foot, and XZ_{gnd} and XZ_{mov} are scale factor matrices. These matrices are given by

$$A = \begin{bmatrix} 0 & 0 & 0 & 0 & 1.0263E-2 & 2.49033E-1 \\ 0 & 0 & 0 & -1.58826E-4 & 7.8736E-3 & 8.97685E-1 \\ 0 & 0 & -1.567E-5 & 1.21278E-3 & -1.4623E-3 & 2.652E-3 \\ -1.80869E-8 & 2.08426E-6 & -7.45788E-5 & 5.85999E-4 & 9.54539E-3 & -2.50062E-4 \end{bmatrix}$$

$$G_{\text{gnd}} = \begin{bmatrix} S\%^5 \\ S\%^4 \\ S\%^3 \\ S\%^2 \\ S\% \\ 1 \end{bmatrix} \quad XZ_{\text{gnd}} = \begin{bmatrix} X_{\text{S}} & 0 & 0 & 0 \\ 0 & Z_{\text{L}} & 0 & 0 \\ 0 & 0 & 0 & 0 \\ 0 & 0 & 0 & 0 \end{bmatrix},$$

$$G_{\text{mov}} = \begin{bmatrix} (S\%-50)^5 \\ (S\%-50)^4 \\ (S\%-50)^3 \\ (S\%-50)^2 \\ (S\%-50) \\ 1 \end{bmatrix} \quad XZ_{\text{mov}} = \begin{bmatrix} X_{\text{S}} & 0 & 0 & 0 \\ 0 & Z_{\text{L}} & 0 & 0 \\ 0 & 0 & X_{\text{S}} & 0 \\ 0 & 0 & 0 & Z_{\text{L}} \end{bmatrix},$$

where $S\%$ represents the gait cycle percentage and takes values from 0 to 50 in the G_{gnd} vector (grounded foot) and values from 50 to 100 in the G_{mov} vector (moving foot). Fig. 3 shows the hip and ankle trajectories of the grounded foot of the biped robot, for a step length $X_{\text{S}} = 0.07$ m and a leg height $Z_{\text{L}} = 0.23$ m (X_{ankle} and Z_{ankle} are zero). Fig. 4 shows the corresponding hip and ankle trajectories of the moving foot.

The trajectory of the human torso was obtained, and it was verified that the torso angle trajectory of some human walks can be approximated by a cosine function.[45] The amplitude (M) of this trajectory is determined by simulation of the

https://doi.org/10.1017/S0263574710000627 Published online by Cambridge University Press

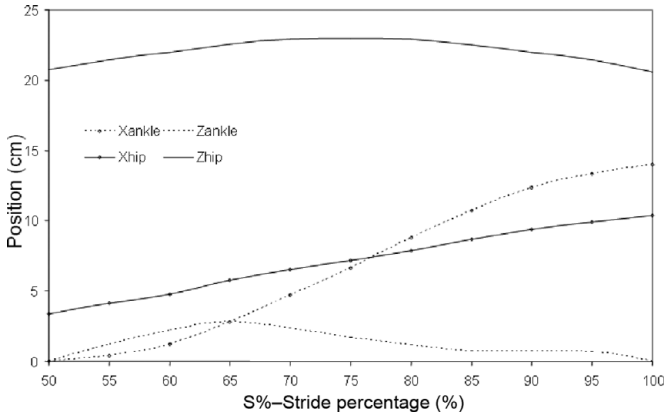

Fig. 4. Hip and ankle trajectories of the moving foot.

biped robot in order to have the ZMP located at the center of the grounded foot at the beginning of the swing phase (that coincides with the end of the double phase). This amplitude cannot be the same of the human's, because our robot has neither head nor arms and the mass distribution is different. The designed torso angle trajectory was then chosen to be given by

$$\theta_{\text{torso}} = \begin{cases} M\cos\left(\dfrac{2\pi S\%}{100}\right), & \text{if } 0 < S\% < 50 \\ M\cos\left(\dfrac{2\pi(S\% - 50)}{100}\right), & \text{if } 50 < S\% < 100 \end{cases}, \tag{3}$$

where $M = X_{1\text{CoM}}K(t_{\text{step}})$. The constant $X_{1\text{CoM}}$ is equal to the X coordinate of the center of mass (CoM) (X_{CoM}) in the double phase, with the torso vertical. During the double phase $S\%$ is constant (equals 0, 50, or 100) and the torso angle changes from $-$M to M or from M to $-$M. At the same time, the pendulum moves to the opposite side (from left to right or vice versa). During the swing phase, the $S\%$ is proportional to time. The X coordinate system axis is pointing forward, and its origin is in the center of the grounded foot. $K(t_{\text{step}})$, where t_{step} is the time duration of the step, is the dynamic torso angle correction for one unit length of X_{ZMP} deviation (9) and will be presented in Section 4. The ground projection of the CoM can be calculated in real time as

$$X_{\text{CoM}} = \frac{\sum_{i=0}^{7} m_i g x_i}{\sum_{i=0}^{7} m_i g}, \tag{4}$$

$$Y_{\text{CoM}} = \frac{\sum_{i=0}^{7} m_i g y_i}{\sum_{i=0}^{7} m_i g}, \tag{5}$$

where m_i is the mass of the link i and g is the gravity acceleration. X_{CoM} is used instead of X_{ZMP} to avoid the ZMP calculation, which can only be done offline due to its large processing time.

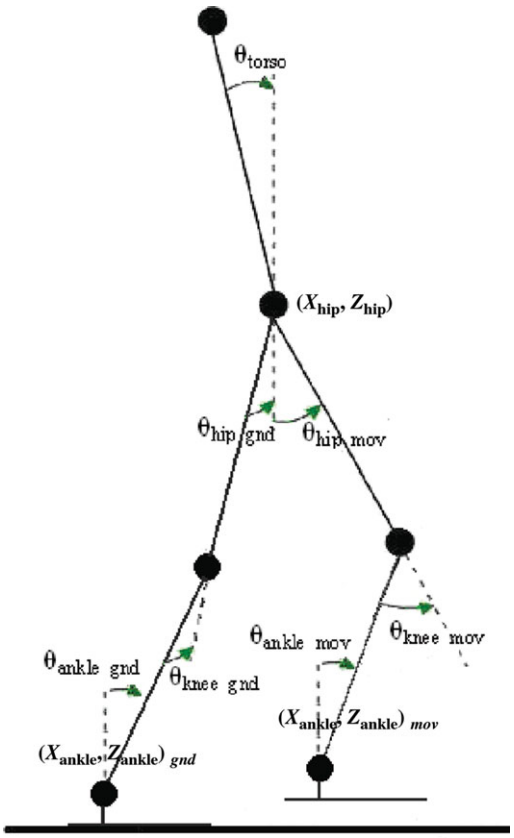

Fig. 5. Biped model with joint angles description.

The trajectories described above were also used for walking on slopes after applying a rotation matrix R to the hip and ankle Cartesian trajectories (6), and adding the slope angle θ to the ankle's joint angles so that the whole robot is tilted.

$$\begin{bmatrix} X_{\text{hip}} \\ Z_{\text{hip}} \\ X_{\text{ankle}} \\ Z_{\text{ankle}} \end{bmatrix}_{\text{slope}} = R \begin{bmatrix} X_{\text{hip}} \\ Z_{\text{hip}} \\ X_{\text{ankle}} \\ Z_{\text{ankle}} \end{bmatrix}_{\text{horizontal}}. \tag{6}$$

with

$$R = \begin{bmatrix} \cos\theta & -\sin\theta & 0 & 0 \\ \sin\theta & \cos\theta & 0 & 0 \\ 0 & 0 & \cos\theta & -\sin\theta \\ 0 & 0 & \sin\theta & \cos\theta \end{bmatrix}.$$

Using inverse kinematics, all relevant joint angles of the biped model presented in Fig. 5 are calculated.

3.2. Joint trajectories based on neural network

Using the above trajectories and inverse kinematics, the joint angles' trajectories were obtained and used for training a FF backpropagation neural network, which is used to generate the gait of the biped robot. This network has four inputs (step length, step time, slope inclination, and percentage of the gait cycle) and seven output angles:

https://doi.org/10.1017/S0263574710000627 Published online by Cambridge University Press

Table I. Physical characteristics of the biped robot.

Biped	Mass (kg)	Length (m)	$I_x(\times 10^{-4}\text{kg}\cdot\text{m}^2)$	$I_y(\times 10^{-4}\text{kg}\cdot\text{m}^2)$
Foot	0.28×2	0.035	2.64	3.51
Shank	0.15×2	0.115	7.23	6.81
Thigh	0.15×2	0.115	7.23	6.81
Haunches	0.60	0.065	21.25	9.70
Pendulum	0.54	0.170	159.58	160.17

$\theta_{\text{ankle\_gnd}}$, $\theta_{\text{knee\_gnd}}$, $\theta_{\text{hip\_gnd}}$, $\theta_{\text{hip\_mov}}$, $\theta_{\text{knee\_mov}}$, $\theta_{\text{ankle\_mov}}$, and θ_{lateral}.θ_{torso} value is defined by $\theta_{\text{hip\_gnd}}$ and $\theta_{\text{hip\_mov}}$.

This network was first trained with 251 and then tested with 64 uniformly distributed and normalized datasets. Mean square errors (MSE) lower than 0.00001 and 0.001 were needed, respectively, for training and testing. Levenberg–Marquardt optimization was used to update the weight and bias values of the network. The application of this method requires a good balance between overfitting and underfitting to obtain smooth joint angle behavior.

An FF network with two hidden layers with 24 neurons each was chosen, after some simulations with different configurations. The transfer functions for the hidden layers are sigmoid functions and for the output layer they are linear functions. The MSE obtained were 0.0000097 and 0.00066 for training and test data, respectively. This FF network is able to predict the entire sequence of the gait with step lengths between 0.04 m and 0.12 m and slope inclinations between -10 degrees and $+10$ degrees. The use of this FF network rather than the direct use of the previous subsection equations will allow the future use of RL techniques.

4. Torso Trajectory Planning Simulation Algorithm

The method used to obtain the balance of the robot in the sagittal plane consists of correcting the torso angle (actuating the hip joints) using the SVR or the NF real-time output. Balance in the lateral plane is achieved by positioning the pendulum (θ_{lateral}) at its extreme lateral positions during the single phase. This way Y_{zmp} is neglected. Both the SVR and the NF were trained with 239 uniformly distributed and normalized data points and tested with another 68 data points, generated by simulation, as described next. The ZMP location, which is the balance control variable, is calculated by the following expressions,[11] given the robot mass model of Fig. 6 and the physical characteristics presented in Table I.

$$X_{zmp} = \frac{\sum_{i=0}^{7} m_i(\ddot{z}_i + g)x_i - \sum_{i=0}^{7} m_i\ddot{x}_i z_i - \sum_{i=0}^{7} I_{iy}\alpha_{iy}}{\sum_{i=0}^{7} m_i(\ddot{z}_i + g)}, \quad (7)$$

$$Y_{\text{zmp}} = \frac{\sum_{i=0}^{7} m_i(\ddot{z}_i + g)y_i - \sum_{i=0}^{7} m_i\ddot{y}_i z_i + \sum_{i=0}^{7} I_{ix}\alpha_{ix}}{\sum_{i=0}^{7} m_i(\ddot{z}_i + g)}. \quad (8)$$

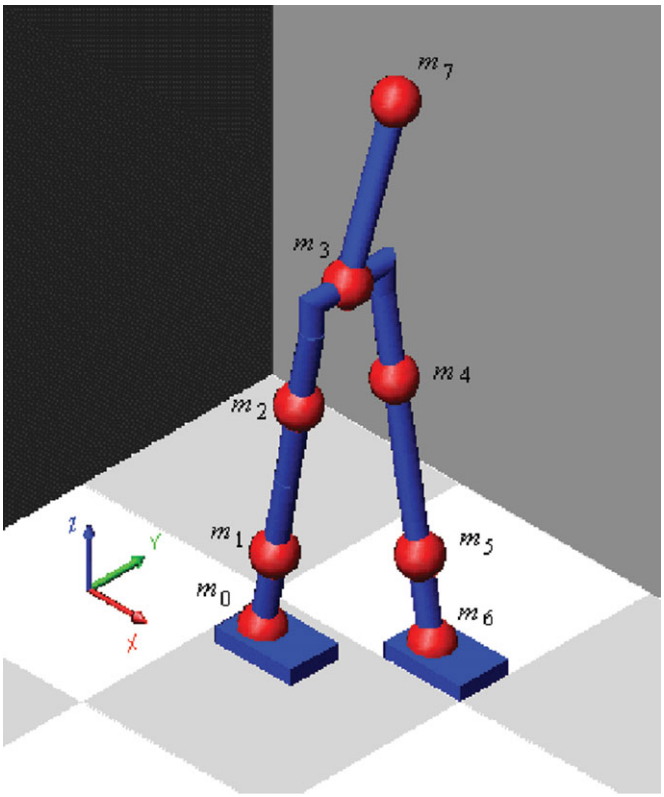

Fig. 6. Biped eight-link mass model.

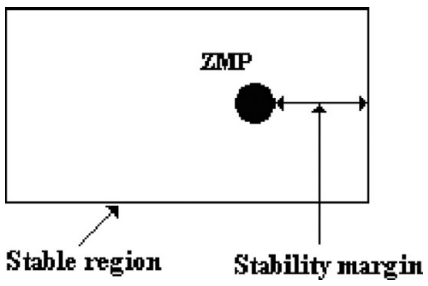

Fig. 7. Definition of the stability margin.

$\ddot{x}$, $\ddot{y}$, and $\ddot{z}$ are linear accelerations, I_{ix} and I_{iy}, are inertia coefficients, α_{ix} and α_{iy} are angular accelerations, m_i is the mass of the link i, and g is the gravity acceleration.

The stability margin is the minimum distance between the ZMP and the border of the stable region and can be considered as an indicator of the quality of the robot's stability (Fig. 7). If the robot is in the swing phase (only one foot on the ground) the stable region consists of the area of contact of the foot on the ground. In the double phase, the stable region is a polygon inscribing the contact areas of the

https://doi.org/10.1017/S0263574710000627 Published online by Cambridge University Press

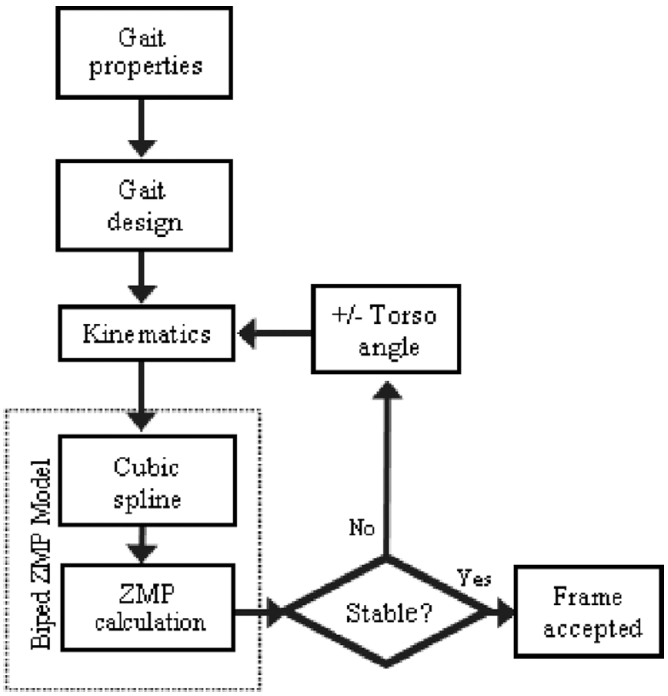

Fig. 8. Torso trajectory planning simulation algorithm.

two feet. If the ZMP remains inside the stable region it can be said that the biped robot's walking is stable. When the stability margin is large, that is, when the ZMP is next to the center of the stable region, it can be said that the biped robot exhibits a high stability.

It is described next the torso trajectory planning simulation algorithm. It is executed offline, generating data used for the SVR and the NF training. First, taking into account the gait's characteristics (step length and step time), thirteen via-points (7) for the swing phase and 6 for the double phase) of the ankle and hip trajectories are obtained using (6), (1), and (2) for one step. After that, the trajectories of all joints are calculated using inverse and direct kinematics and cubic splines are generated for each of these trajectories. Next, the X_{ZMP} is calculated by (7) and the stability margin is determined. The stability margin is then used to make iterative corrections to the torso angle, using the desired X_{ZMP} (which is the center of the grounded foot) as reference, until a predefined stability margin is reached. This procedure is repeated for all 13 frames of the step. Fig. 8 shows the algorithm just explained. This algorithm is executed for 50 steps (5 different lengths and 10 different step times).

With this algorithm, four splines (x, y, z linear accelerations and angular acceleration) are needed for each link, resulting in a high computational effort and making the real-time computation difficult. So, these planned trajectories are used to train the NF network and the SVR, which are then used for the real-time control of the torso of the robot.

Another result of the simulation is the relation $K(t_{step})$ between the torso angle correction ($\Delta\theta_{Torso}$) and the X_{ZMP} error (difference between the actual X_{ZMP} and X_{ZMPD}, the desired X_{ZMP}) (see Fig. 9). In this case X_{ZMPD} is zero, because it is the origin of the coordinate system. The $K(t_{step})$ function is used to design the trajectory of the torso angle, using (3).

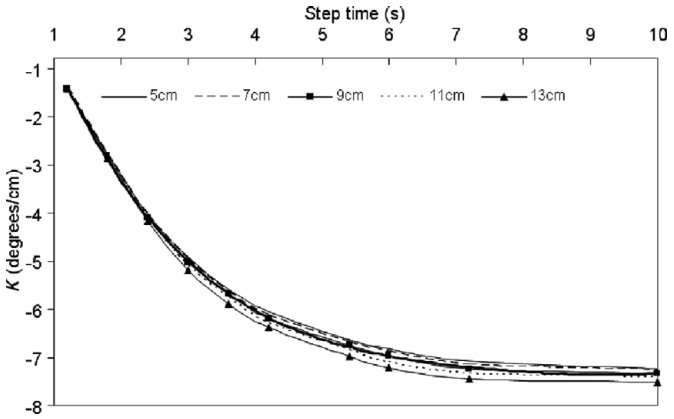

Fig. 9. The relation $K(t_{step}) = \Delta\theta_{Torso}/(X_{ZMP} - X_{ZMPD})$.

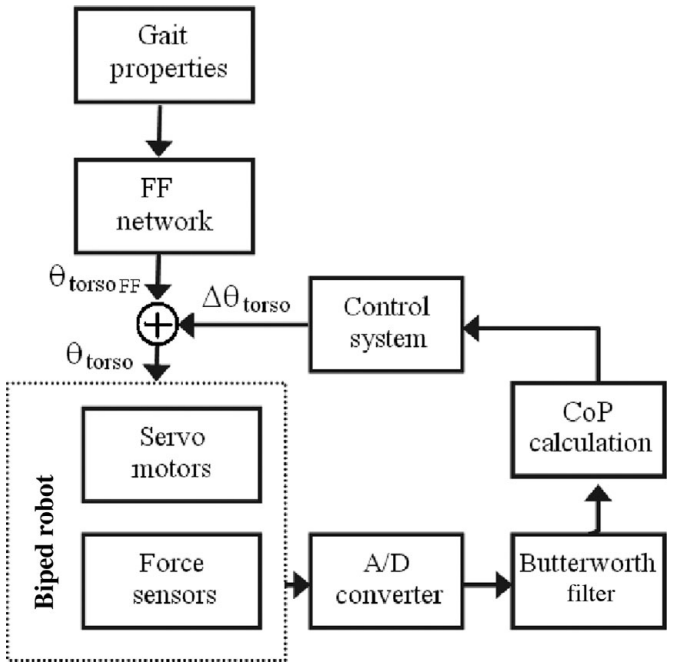

Fig. 10. Balance control strategy of the biped robot.

Analyzing Fig. 9, it is possible to conclude that $K(t_{step})$ is almost independent of the length of the step, depending on the step time. Using a curve fitting algorithm the function

$$K(t_{step}) = 0.002t_{step}^4 - 0.0637t_{step}^3 + 0.7795t_{step}^2 - 4.4803t_{step} + 2.7866 \quad (9)$$

was obtained, where t_{step} is the step time of the gait (half-stride time).

5. Real-Time Control Strategy

The control strategy is one of the most important issues in controlling a biped robot. Many control strategies are available, based on fuzzy systems, neural networks, classic control, support vector machines (SVMs), and hybrid systems. The main blocks of the biped robot control are presented in Fig. 10. The control system block is implemented by an SVR controller or by an NF controller,

https://doi.org/10.1017/S0263574710000627 Published online by Cambridge University Press

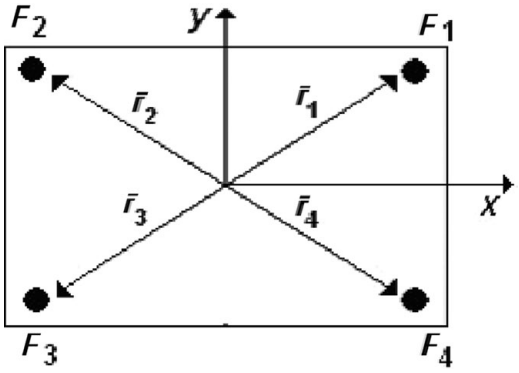

Fig. 11. Top view of the location of the force sensors under the foot.

both described in Section 6. In order to allow real-time control, the actual (real) value of the ZMP is needed. When the ZMP is within the stable region, the ZMP is equal to the center of pressure (CoP).

To determine the CoP, four force sensors under each foot of the robot are used (see Fig. 11). The CoP is calculated by

$$\mathrm{CoP} = \frac{\sum_{i=1}^{4} F_i \cdot \bar{r}_i}{\sum_{i=1}^{4} F_i}, \tag{10}$$

where F_i is the measured force in sensor i, and $\bar{r}_i$ is the position vector, as defined in Fig. 11.

The force sensors' reading are acquired by an analog to digital converter (ADC) with 10 bits of resolution and a maximum sampling rate of 30 Hz. The force measurements are noisy because the force sensors are sensitive to vibrations during the motion, so a second-order Butterworth low-pass filter is used to remove the high-frequency noise from the force sensor signals. A cutoff frequency of 3 Hz was used. The difference equation for a second-order low-pass Butterworth digital filter has the form:

$$y_k = b_1 x_k + b_2 x_{k-1} + b_3 x_{k-2} - a_2 y_{k-1} - a_3 y_{k-2}, \tag{11}$$

where y is the filtered variable, x is the unfiltered variable, x_k is the value of x at time t_k, y_k is the value of y at time t_k, $t_k = kT$ is the current time, $T = t_k - -t_{k-1}$ is the sampling period, and k is an integer.

6. Intelligent Controllers for Biped Sagittal Balance

Among the computational intelligence techniques available, a TSK first-order NF and a SVR were used and compared. The first computational intelligence technique was chosen because the training data were obtained in a nondeterministic way from the Ziegler–Nichols method, and it is a traditional approach. The second was chosen mainly due to its type of regression and to its fast execution time. Moreover, it is considered the state of the art in computational intelligence techniques, and it has not been used often in the field of biped robotics.

6.1. SVR controller

Support vector machines were first developed by Vapnik[24] to solve classification problems, and then successfully extended to regression and density estimation problems.[27] SVM are gaining popularity due to their many attractive features and promising empirical performance. The formulation of SVM employs the structural risk minimization (SRM) principle, which has been shown to be superior to the traditional empirical risk minimization (ERM) principle employed in conventional learning algorithms (e.g. neural networks).[28] SRM minimizes an upper bound on the generalization error, whereas ERM minimizes the error on the training data. This difference makes SVM more attractive in statistical learning applications. SVM are used for classification and regression. In this work, a regression SVM (an SVR) is used.

- SVR

Given a set of data points, $(x_1, z_1), \ldots, (x_k, z_k)$, such that $x_i \in R^n$ is an input vector and $z_i \in R$ is a target output, the standard form of SVR[24] is

$$\min_{w,b,\xi,\xi^*} \quad \frac{1}{2} w^T w + C \sum_{i=1}^{k} \xi_i + C \sum_{i=1}^{k} \xi_i^* \tag{12}$$

$$\text{subject to } w^T \phi(x_i) + b - z_i \le \varepsilon + \xi_i,$$
$$z_i - w^T \phi(x_i) - b \le \varepsilon + \xi_i^*,$$
$$\xi_i, \xi_i^* \ge 0, \quad i = 1, \ldots, k.$$

Its dual is

$$\min_{\alpha,\alpha^*} \quad \frac{1}{2}(\alpha - \alpha^*)^T Q(\alpha - \alpha^*) + \varepsilon \sum_{i=1}^{k} (\alpha_i + \alpha_i^*) \tag{13}$$
$$+ \sum_{i=1}^{k} z_i(\alpha_i - \alpha_i^*)$$
$$\text{subject to } \sum_{i=1}^{l} (\alpha_i - \alpha_i^*) = 0,\ 0 \le \alpha_i, \alpha_i^* \le C,$$
$$i = 1, \ldots, k,$$

where $Q_{ij} = k(x_i, x_j) \equiv \phi(x_i)^T \phi(x_j)$.

The approximate function is

$$f(x) = \sum_{i=1}^{k} (-\alpha_i + \alpha_i^*) k(x_i, x) + b. \tag{14}$$

To solve this problem, the Gaussian kernel

$$k(x_i, x_j) = \exp(-\gamma ||x_i - x_j||^2) = \exp\left(-\frac{(x_i - x_j)^2}{2\sigma^2}\right) \tag{15}$$

was used.

Figure 12 shows the insensitive band (tube) of a typical nonlinear regression function when the SVR method is used.

The LIBSVM[29] was used to solve the SVR with the chosen kernel. C, ε and γ parameters of (12) to (15) must be carefully

https://doi.org/10.1017/S0263574710000627 Published online by Cambridge University Press

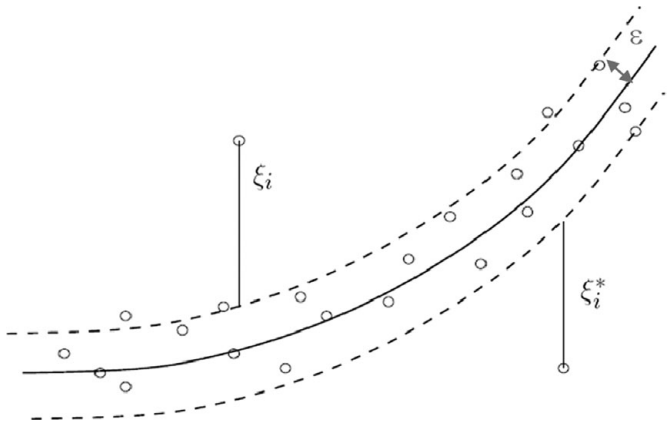

Fig. 12. The insensitive band for a nonlinear regression function.

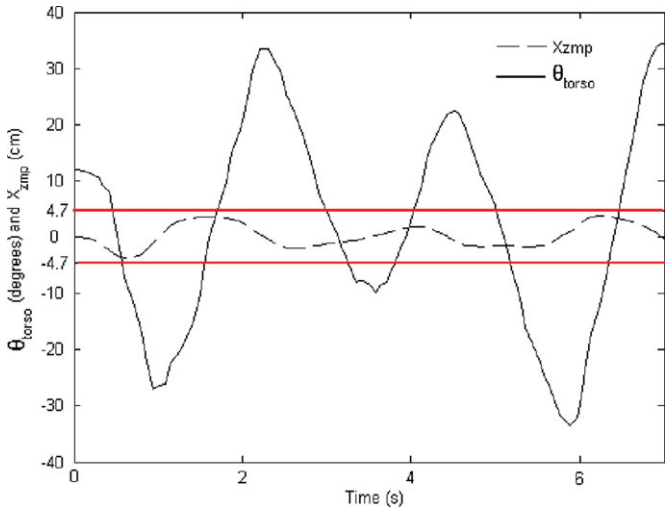

Fig. 13. X_{ZMP} and θ_{torso} when the robot has one foot on the ground, with the proportional controller active, using the critical proportional gain.

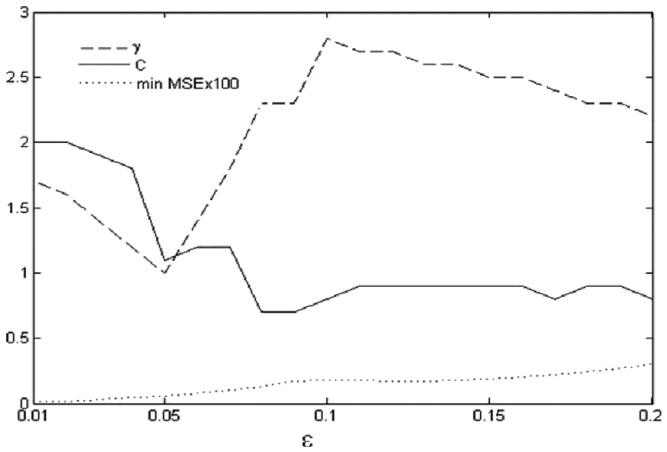

Fig. 14. γ, C, and MSE against ε.

chosen to generate the best model. Parameter C symbolizes the importance of the values (ξ_i and ξ_i^*) outside the regression tube, ε corresponds to the radius of the regression function tube, and γ represents the Gaussian kernel width. Therefore, the number of support vectors is a decreasing function of ε and a nonzero value of ε is required to avoid overfitting. On the other hand, a too large value of ε could result in underfitting.

6.1.1. Offline training of SVR controller. The SVR input variables are the X_{ZMP} and DX_{ZMP}. X_{ZMP} is the x coordinate of the ZMP and $\mathrm{DX}_{\mathrm{ZMP}}$ is its time derivative. The SVR output is the torso angular correction ($\Delta\theta_{\mathrm{torso}}$), which is applied to the two hip joints. The training data are the $\Delta\theta_{\mathrm{torso}}$, the X_{ZMP} and $\mathrm{DX}_{\mathrm{ZMP}}$. The $\Delta\theta_{\mathrm{torso}}$ versus X_{ZMP} training data were obtained by simulation, as described in Section 4. The $\Delta\theta_{\mathrm{torso}}$ versus $\mathrm{DX}_{\mathrm{ZMP}}$ data were obtained through the Ziegler–Nichols method,[30] having a PD controller in mind. In fact, for the biped robot system, the easiest way to determine the proportional and derivative controller parameters is using the second method proposed by Ziegler–Nichols, based on the response of the closed-loop system at the limit of stability. The first step of this method is to determine experimentally the value of the critical proportional gain (K_c), defined as the largest value that the gain of the controller can achieve and that results in a curve of closed-loop response with sustained oscillations when a pure proportional controller is used. The frequency of oscillation is called critical frequency of oscillation (ω_c). Figure 13 shows the result of such an experiment. The value of K_c obtained for the limit of stability was 10.3. Thus, K_p equals 6.2, as $K_p = 0.6 \times K_c$. The derivative parameter (K_d) of the PD controller is then calculated using the relationship $K_d = K_p\pi/(4\omega_c)$. The critical frequency of oscillation (ω_c) is equal to 2.7rad/s, leading to K_d equal to 1.8. Using (9) and making $K(t_{\mathrm{step}})$ equal to K_p results in a 4 s step time. This was the step time chosen for data training.

In a first step, 34 points (X_{ZMP}, $\Delta\theta_{\mathrm{torso}}$) were obtained by simulation of the biped robot, five steps with seven frames each, excluding the point (X_{ZMP}, $\Delta\theta_{\mathrm{torso}}$) = (0, 0). In a second step, for each of these 34 points, 9 new points were generated with DX_{ZMP} varying uniformly between −0.002 and 0.002 m. These range values were determined by the maximum velocity of the X_{ZMP} occurred in the above experiment, that is, 0.043m/s and by multiplying it by the sampling time ($\Delta t = 0.046$ s). The $\Delta\theta_{\mathrm{torso}}$ for each training and testing point ($\Delta\theta_{\mathrm{torso\,PD}_k}$) was obtained by

$$\Delta\theta_{\mathrm{torsoPD}_k} = \Delta\theta_{\mathrm{torso}_k}(X_{\mathrm{ZMP}_k}) + k_d DX_{\mathrm{ZMP}_k}/\Delta t.$$

This way 307($34 \times 9 + 1$) points were obtained, 239($34 \times 7 + 1$) points for training, and 68(34×2) for testing. The values used were normalized, dividing $\Delta\theta_{\mathrm{torsoPD}k}$ by 45°, X_{zmp} by 0.06 m, and $\mathrm{DX}_{\mathrm{zmp}}$ by 0.002 m.

To choose the SVR parameters, ε was varied from 0.01 to 0.2, C was varied from 0.1 to 2, and γ from 1 to 4. Fig. 14 shows the minimum MSE as a function of ε as well as the corresponding C and γ parameters.

As the number of support vectors is a decreasing function of ε, a big ε must be chosen in order to minimize the number of support vectors (to speed up computation). On other hand a small MSE must be obtained. The value $\varepsilon = 0.13$ was chosen from the plot of MSE against ε (see Fig. 14) because it is the largest ε in the region $0.09 \leq \varepsilon \leq 0.13$ where the MSE is approximately constant and small (equals 0.0017). For this value of ε the other parameters are taken from Fig. 14 as

https://doi.org/10.1017/S0263574710000627 Published online by Cambridge University Press

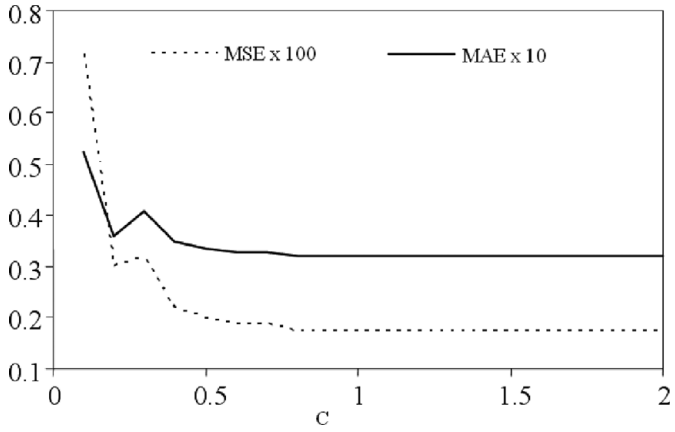

Fig. 15. MSE and MAE against C (for $\varepsilon = 0.13$ and $\gamma = 2.6$).

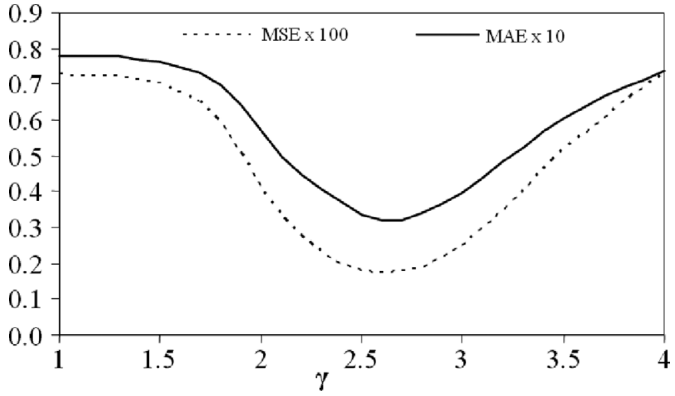

Fig. 16. MSE and MAE against γ (for $\varepsilon = 0.13$ and $C = 0.9$).

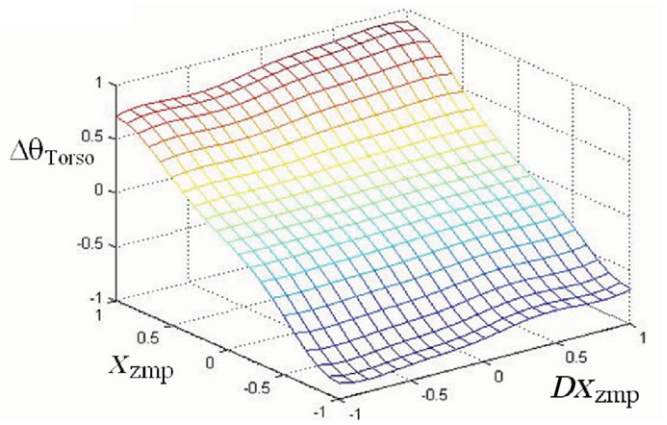

Fig. 17. SVR output (normalized values).

$\gamma = 2.6$ and $C = 0.9$. Figures 15 and 16 show the variation of the MSE and the mean absolute error (MAE) versus C and γ, respectively, confirming the correct choice of the parameters.

The execution time of this SVR is about 0.2 ms (on a 3 GHz PC), which is adequate for the real-time balance control of the biped robot. Fig. 17 shows the SVR output.

6.2. *Neural-fuzzy controller*

The proposed NF network is a first-order Takagi–Sugeno–Kang type[26] with two antecedents, one consequent, and seven membership functions. With three and five membership functions, the behavior is not so smooth and the error is bigger. The antecedent variables are again the X_{ZMP} and DX_{ZMP}. The net output (the consequent), $\Delta\theta_{\mathrm{torso}}$, is the torso angular correction. The seven linguistic antecedent terms are: negative big (NB), negative medium (NM), negative small (NS), zero (ZE), positive big (PB), positive medium (PM), and positive small (PS).

Table II. Quadratic error of the NF system.

Type of membership function	MSE
Triangular	0.004138
Gaussian	0.003876
Sigmoid	0.003308

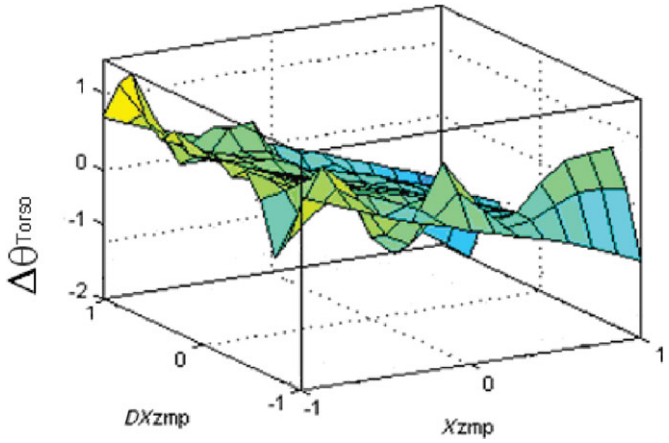

Fig. 18. Variation of the torso correction angle obtained with the NF network using triangular membership functions.

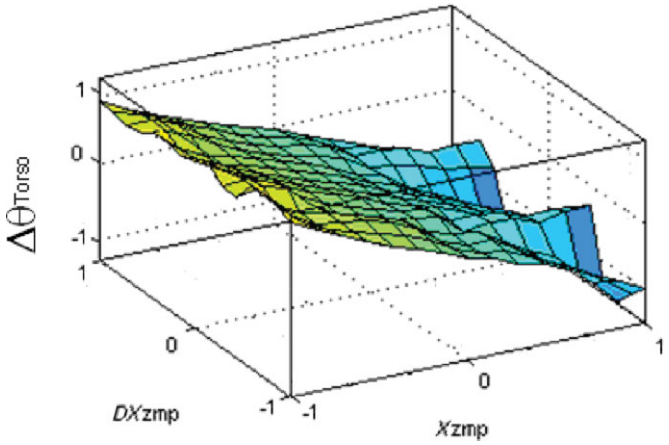

Fig. 19. Variation of the torso correction angle obtained with the NF network using Gaussian membership functions.

6.2.1. Offline training of neural-fuzzy controller. The same set of 239 and 68 normalized data points were used for training and for tests, respectively, as with the SVR. In order to choose the type of membership functions to use, triangular, Gaussian, and sigmoid functions were simulated. The MSE and the behavior of the network in the range of the training values were compared. The results are presented in Table II and in Fig. 18–20 (normalized values).

After analyzing the figures and the table obtained it is possible to conclude that the most suitable membership

https://doi.org/10.1017/S0263574710000627 Published online by Cambridge University Press

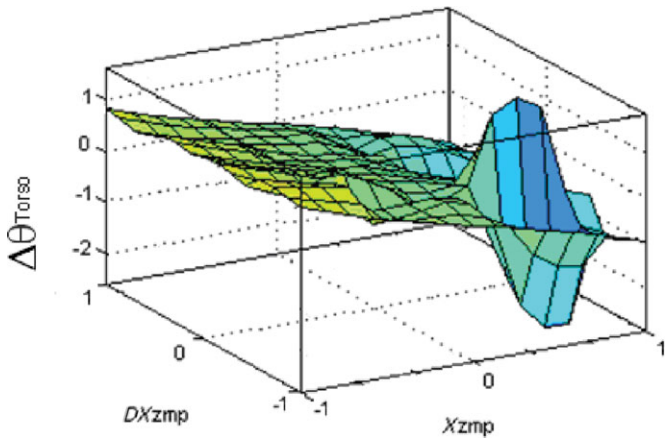

Fig. 20. Variation of the torso correction angle obtained with the NF network using sigmoid membership functions.

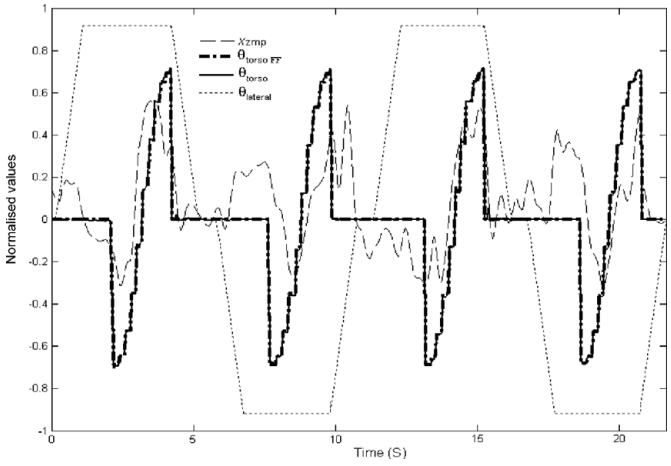

Fig. 21. X_{zmp}, FF generated torso (θ_{torsoFF}), torso (θ_{torso}), and lateral (θ_{lateral}) angles obtained with the robot walking on a flat horizontal surface without torso control.

function for this system is the Gaussian. Although it does not have the least quadratic error, its behavior is smoother. As the execution time of the NF network is less than 10 ms, the real-time control of the biped robot is possible.

7. Experimental Results

To test and compare the performances of the control systems based on the SVR and on the NF, seven experiments were performed, for a step length of 0.12 m. The results of these experiments are shown in the figures below. The values shown were normalized by dividing the data values by 25° for θ_{torso}, by 55° for θ_{lateral} and by 0.047 m for X_{zmp}. All the experiments were performed with a swing phase equal to 2.2 s and with the $X_{\text{zmp\_ref}}$ (X_{zmp} reference) equal to zero (corresponding to the center of the foot, see Fig. 11).

In the first experiment, the biped robot walked on a flat horizontal surface without the torso controller active, using the torso angle value generated by the FF net. Fig. 21 shows the X_{zmp} behavior. It can be seen that the robot never falls, although the X_{zmp} is not close to zero.

In the second and third experiments, the robot walked on a flat horizontal surface with, respectively, the SVR and

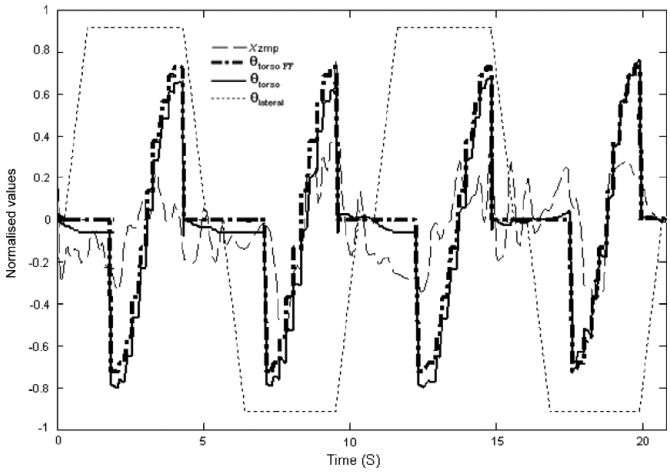

Fig. 22. X_{zmp}, FF generated torso (θ_{torsoFF}), torso (θ_{torso}), and lateral (θ_{lateral}) angles obtained with the SVR controller with the robot walking on a flat horizontal surface.

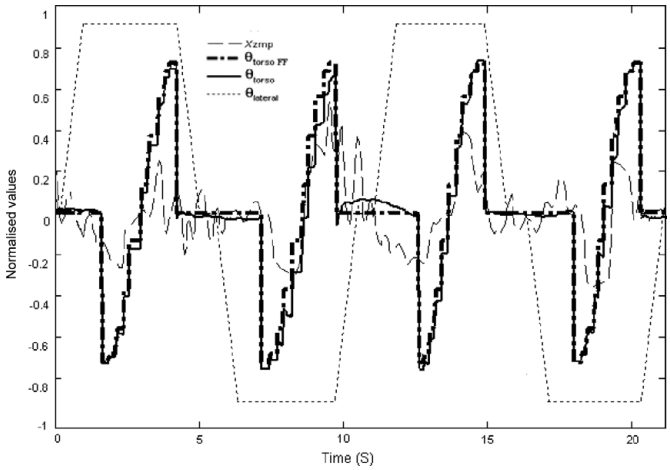

Fig. 23. X_{zmp}, FF generated torso (θ_{torsoFF}), torso (θ_{torso}), and lateral (θ_{lateral}) angles obtained with the NF controller with the robot walking on a flat horizontal surface.

NF torso balance controller active. The X_{zmp} behavior is now closer to zero (see Fig. 22 and Fig. 23) increasing the stability margin. Both the torso angle value generated by the FF (θ_{torsoFF}) and the torso angle value corrected by the SVR or NF controller (θ_{torso}) are plotted. These plots show the effectiveness of these controllers, as the values of X_{zmp} are lower than those in Fig. 21, where the controller is inactive.

In the fourth and fifth experiments, the biped robot walked on an up slope with a 10° inclination with, respectively, the SVR and the NF controllers active. The X_{zmp} behavior is closer to zero, as in the previous experiments (see Fig. 24 and Fig. 25).

In the sixth and seventh experiments, the biped robot walked on a down slope with a 10° inclination with, respectively, the SVR and the NF controllers active. The X_{zmp} behavior is closer to zero, as in the previous experiments (see Fig. 26 and Fig. 27).

To analyze which is the best controller, and because the plots are inconclusive, two performance indexes are proposed. The first is the root of the mean squared of the normalized $X_{\text{ZMP}} - -X_{\text{ZMP\_ref}}$ (NX_{RMS}); the second is the mean

https://doi.org/10.1017/S0263574710000627 Published online by Cambridge University Press

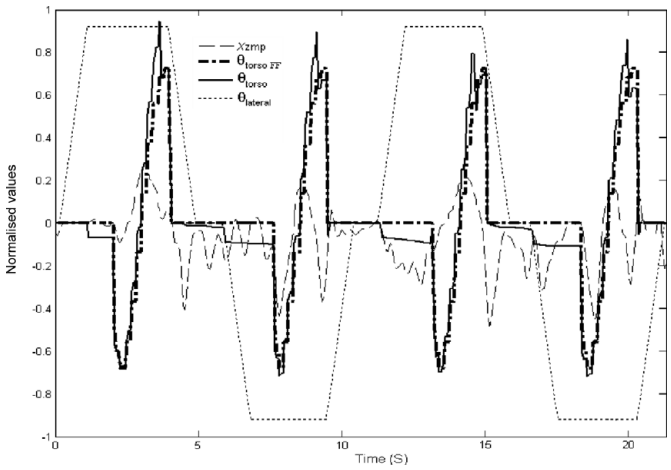

Fig. 24. X_{zmp}, FF generated torso ($\theta_{torsoFF}$), torso (θ_{torso}), and lateral ($\theta_{lateral}$) angles obtained with the SVR controller with the robot walking on an up slope.

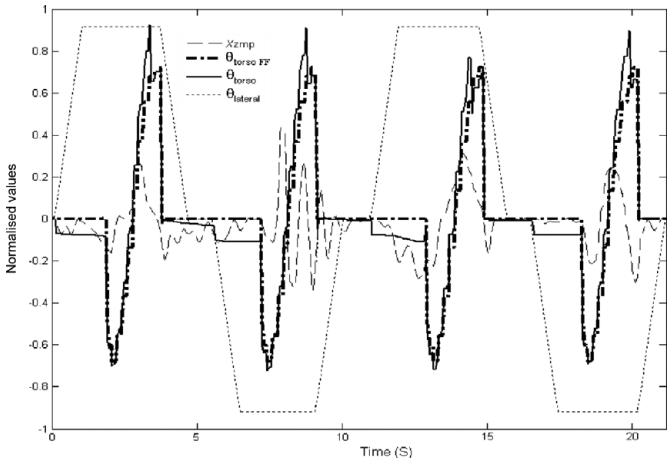

Fig. 25. X_{zmp}, FF generated torso ($\theta_{torsoFF}$), torso (θ_{torso}), and lateral ($\theta_{lateral}$) angles obtained with the NF controller with the robot walking on an up slope.

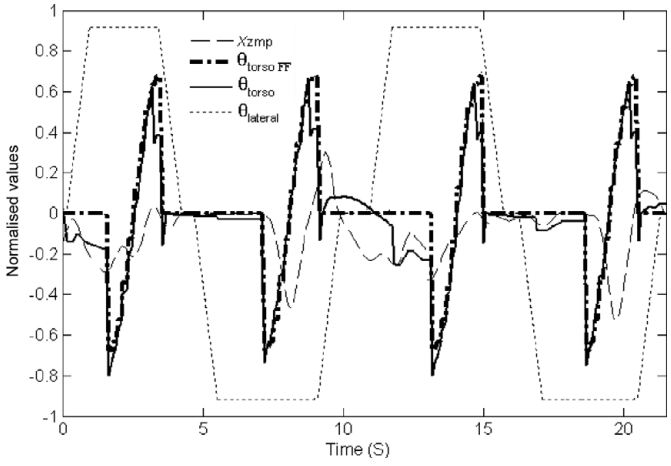

Fig. 26. X_{zmp}, FF generated torso ($\theta_{torsoFF}$), torso (θ_{torso}), and lateral ($\theta_{lateral}$) angles obtained with the SVR controller with the robot walking on a down slope.

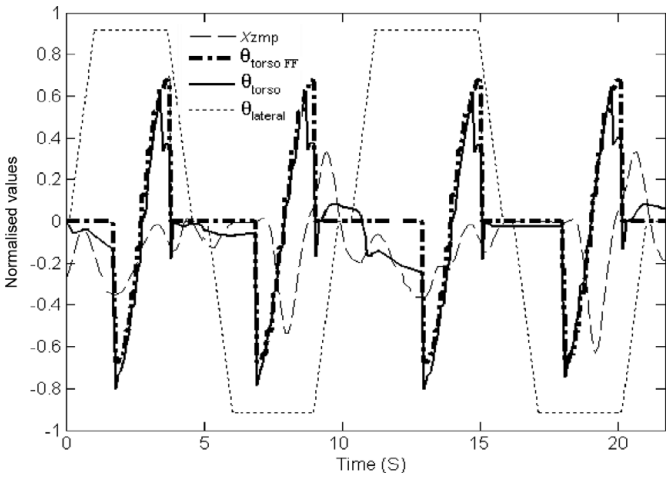

Fig. 27. X_{zmp}, FF generated torso ($\theta_{torso\ FF}$), torso (θ_{torso}), and lateral ($\theta_{lateral}$) angles obtained with the NF controller with the robot walking on a down slope.

Table III. Performance indexes.

Slope	Controller	NX_{RMS}	MNSM
0	None	0.336	0.726
0	SVR	**0.228**	0.819
	NF	0.231	**0.840**
10	SVR	**0.241**	**0.830**
	NF	0.243	0.805
−10	SVR	**0.240**	**0.833**
	NF	0.276	0.810

of the normalized stability margin (MNSM). These indexes were calculated during four walking steps and are described by

$$NX_{\mathrm{RMS}} = \frac{\frac{1}{k}\sum_{i=1}^{k}\sqrt{\frac{1}{n}\sum_{j=1}^{n}(X_{\mathrm{ZMP}}(i,j) - X_{ZMP\_ref}(j))^2}}{X_{\mathrm{S}}}, \quad (16)$$

$$\mathrm{MNSM} = \frac{\frac{1}{k}\sum_{i=1}^{k}\frac{1}{n}\sum_{j=1}^{n}(X_{\mathrm{S}} - |X_{\mathrm{ZMP}}(i,j)|)}{X_{\mathrm{S}}}, \quad (17)$$

where k is the number of steps, n is the number of the force sensor samples and X_S is the X absolute coordinate of the force sensors' locations, which corresponds to the maximum possible value of X_{zmp} (in the present robot this is 0.047 m). The optimal value for NX_{RMS} is zero, and for MNSM it is one.

Table III presents the two performance indexes for the experiments. The values presented in bold are the best ones. Analyzing this table, it is possible to conclude that the SVR controller is a little better overall than the NF controller.

The typical execution time is 0.2 ms for the SVR controller and 10 ms for the NF controller.

To confirm the robustness of the balance control system based on an SVR, two other experiments were performed

https://doi.org/10.1017/S0263574710000627 Published online by Cambridge University Press

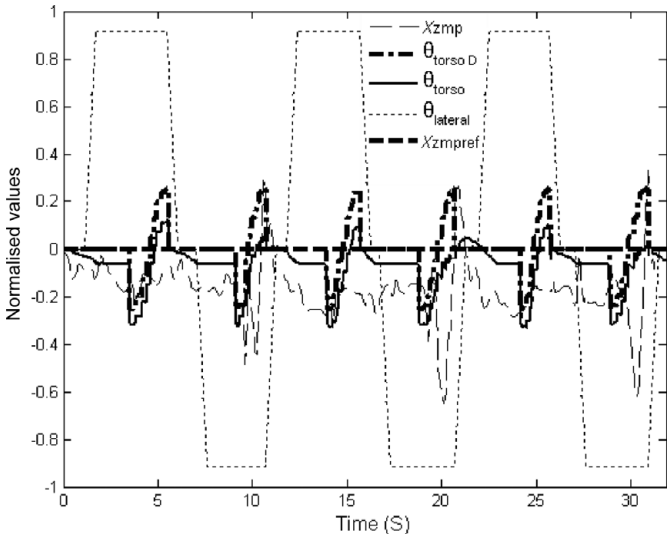

Fig. 28. X_{ZMP}, X_{ZMPref}, designed torso (θ_{torsoD}), torso and lateral angles obtained with the SVR control active with the robot walking on a horizontal flat surface pulling a 1.5 kg mass.

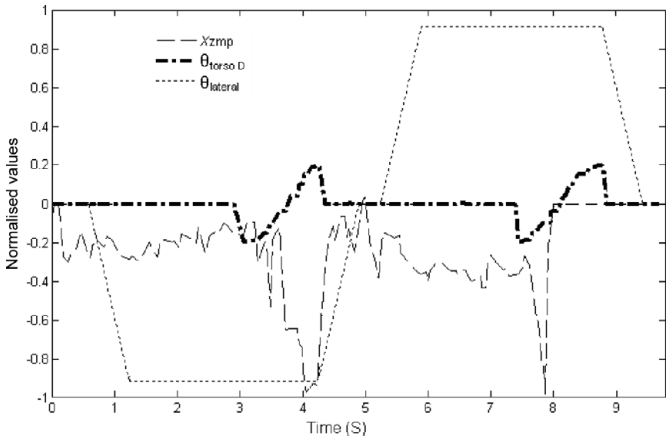

Fig. 30. X_{ZMP}, designed torso (θ_{torsoD}) and lateral angles with the robot walking on a horizontal flat surface, pulling a 1.5 kg mass, without active control.

with the robot dragging a mass. The values presented in the next figures were normalized such that unit values correspond to 25° for θ_{torso}, 10° for θ_{ankle}, 55° for the pendulum lateral angle ($\theta_{lateral}$), and 0.047 m for X_{ZMP}. In the two experiments, the robot was walking on a flat surface, with a step length of 0.07 m, dragging a mass of 1.5 kg (corresponding to a pulling force of about 5 N), with (Fig. 28 and Fig. 29) and without (Fig. 30 and Fig. 31) the SVR controller active. In Fig. 28, it can be noticed that the θ_{torso} is deviated forward relative to the θ_{torsoD} in order to keep the sagittal balance and X_{ZMP} near zero ($X_{ZMPref} = 0$).

It is visible in Fig. 29 (with SVR balance control active) that the robot is able to pull the mass along the step, i.e., the mass moves forward 0.07 m (step length), while in Fig. 31 (without the balance control active) the mass moves forward only 0.035 m and the robot falls down in the next step. In Fig. 30, it is possible to see that the measured value of X_{ZMP} is in the limit of the stable area (larger values of X_{ZMP} are read as this maximum value). The effectiveness of the SVR control is stated in Fig. 28, where the robot presents a good stability margin, compared to Fig. 30, where the X_{ZMP} profile is irregular and the stability margin is close to zero at time about 4 s and zero at about 8 s, when the robot falls down. In[44] other experiments are presented in which this robot is pushed with a force of about 9.8 N while walking and with a force of about 5.5 N while standing on one foot only. In these experiments, performed with the NF controller, the robot kept its stability.

8. Conclusions

The real-time control of a biped robot using the full dynamic model of the ZMP is very time demanding because of the processing of the corresponding equations. The use of a NF network or an SVR balance controller allows a faster control cycle of the robot. Both control methods were tested and satisfactory results obtained. These controllers use the real ZMP, acquired through force sensors placed under the robot's feet. The biped robot did not fall in any of the experiments, presenting a good stability margin with the balance controller active, demonstrating that the SVR controller and the NF controller are both good solutions for biped robot balance control. The two proposed performance indexes show that the biped robot with the SVR controller presents slightly better stability than with the NF controller. The most important advantage of the SVR is the fact that it is about 50 times faster than the NF. The SVR was also tested with the robot pulling a mass that is about 65% of the robot's mass. This SVR controller can also be applied to the lateral balance control. The use of the FF network to generate the gait rather than the direct use of recorded trajectories will allow the future use of RL techniques for an automatic adjustment of the gait to the

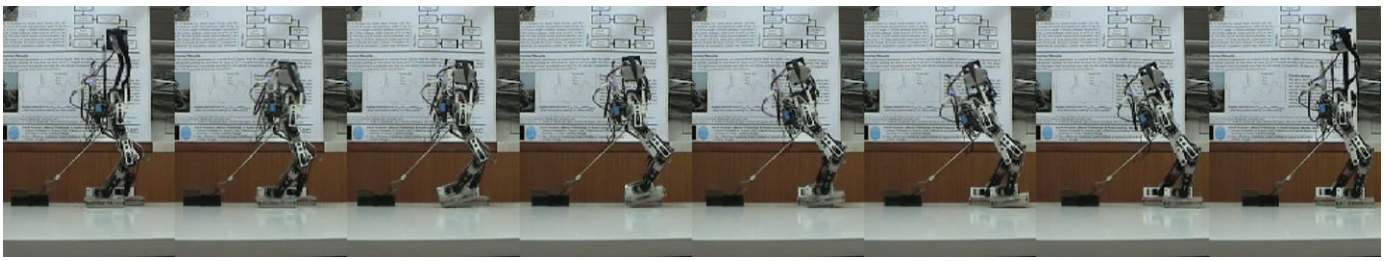

Fig. 29. Walking snapshots of one step on a horizontal flat surface pulling a 1.5 kg mass with the SVR control active.

https://doi.org/10.1017/S0263574710000627 Published online by Cambridge University Press

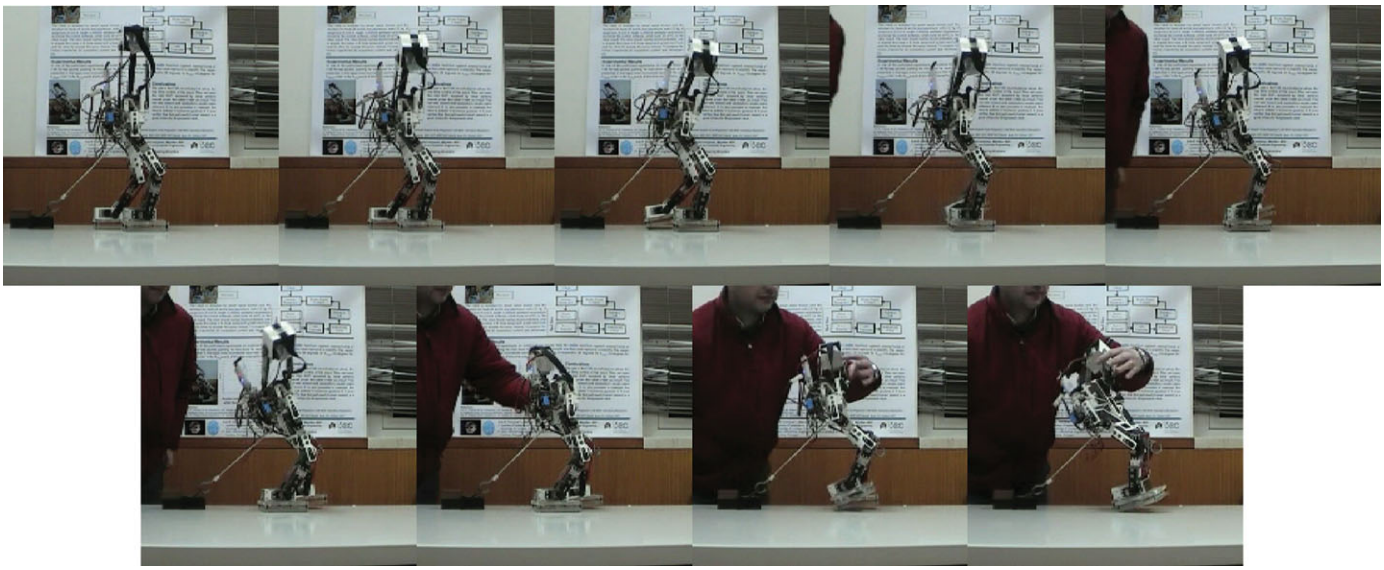

Fig. 31. Walking snapshots on a horizontal flat surface, pulling a 1.5 kg mass without active control. The robot falls down at about $t = 8$ s.

robot and to a changing of the environment, such as walking through grounds with different friction coefficients.

Acknowledgments

The authors would like to thank the Portuguese Fundação para a Ciência e a Tecnologia for financial support.

References

1. Honda Worldwide page. [Online]. Available http://world.honda.com/ASIMO/new/ (18/3/2008).
2. The Humanoid robot research center at KAIST. [Online]. Available http://hubolab.kaist.ac.kr/KHR-3.php (18/3/2008).
3. Biped Humanoid Robot Group – WASEDA. [Online]. Available http://www.takanishi.mech.waseda.ac.jp/research/wabian/index.htm (18/3/2008).
4. Sony page. [Online]. Available http://www.sony.net/SonyInfo/QRIO/top_nf.html (18/3/2008).
5. M. Vukobratović, B. Borovac, D. Surla and D. Stokic, *Biped locomotion: Dynamics, Stability, Control and Application* (Springer-Verlag, Berlin, 1990).
6. M. Nakamura, M. Mori and J. Nishii, "Trajectory Planning for a Leg Swing During Human Walking," *2004 IEEE International Conference on Systems, Man and Cybernetics*, Vol. 1 (Oct. 10–13, 2004), pp. 784–790.
7. J.-H. Yoo, M. S. Nixon and C. J. Harris, "Extracting Human Gait Signatures by Body Segment Properties," *Fifth IEEE Southwest Symposium on Image Analysis and Interpretation (SSIAI'02)* (Apr. 7–9, 2002) pp. 35–39.
8. J. P. Ferreira, M. M. Crisóstomo, A. P. Coimbra, D. Carnide and A. Marto, "A Human Gait Analyzer," *2007 IEEE International Symposium on Intelligent Signal Processing—(WISP'07)*, Madrid, Spain (Oct. 3–5, 2007) pp. 1–5.
9. D. A. Winter, *The Biomechanics and Motor Control of Human Movement*, 2nd ed. (John Wiley & Sons, 1990).
10. K. Hirai, M. Hirose, Y Haikawa and T. Takenaka, "The Development of Honda Humanoid Robot," *Proceedings of the International Conference on Robotics and Automation* (1998) pp. 1321–1326.
11. Q. Huang, S. Kajita, K. Kaneko, K. Yokoi, K. Komoriya and K. Tanie, "A High Stability, Smooth Walking Pattern for a Biped Robot," *Proceedings of the International Conference on Robotics and Automation* (1999) pp. 65–71.
12. I. W. Park, J. Y. Kim, J. Lee and J. H. Oh, "Online Free Walking Trajectory Generation for Biped Humanoid Robot KHR-3(HUBO)," *Proceedings of the 2006 IEEE International Conference on Robotics and Automation*, Orlando, Florida (May 15–19, 2006) pp. 1231–1236.
13. J. Y. Kim, J. Lee and J. H. Oh, "Experimental realization of dynamic walking for a human-riding biped robot, HUBO FX-1," *Adv. Robot.* **21**(3–4), 461–484 (2007).
14. V. Prahlad, G. Dip and C. M. Hwee, "Disturbance Rejection by Online ZMP Compensation," **In**: *Robotica* (Cambridge University Press, 2007) pp. 1–9.
15. K. H. Low, X. Liu, C. H. Goh and H. Yu, "Locomotive control of a wearable lower exoskeleton for walking enhancement," *J. Vib. Control* **12**(12), 1311–1336 (2006).
16. J. H. Park, "Fuzzy-logic zero-moment point trajectory generation for reduced trunk motions of biped robots," *Fuzzy Sets Syst.* **134**, 189–203 (2003).
17. M. Gh. Negoita, D. Kim, N.-H. Kim, S.-J. Seo and G.-T. Park, "Fuzzy Modeling of Zero Moment Point Trajectory for a Biped Walking Robot," *International Conference on Knowledge-Based Intelligent Information and Engineering Systems (KES 2004)* (Lecture Notes in Artificial Intelligence, Vol. 3214), Springer-Verlag, Berlin, Heidelberg (2004) pp. 716–722.
18. K. C. Choi, M. C. Lee and J. M. Lee, "Fuzzy Posture Control for a Biped Walking Robot Based on Force Sensor for ZMP," *The 11th International Symposium on Artificial Life and robotics 2006 (ISAROB ´06)*, Oita, Japan (Jan. 23–25, 2006) pp. 1185–1189.
19. J. P. Ferreira, T. G. Amaral, V. F. Pires, M. M. Crisóstomo and A. P. Coimbra, "A Neural-Fuzzy Walking Control of An Autonomous Biped Robot," *Proceedings of the 10th International Symposium on Robotics with Applications, IEEE CNF*, Seville, Vol. 15 (June 21–23, 2004) pp. 253–258.
20. D. Sim, J. Seo and G. T. Park, "Zero moment point trajectory modeling of a biped walking robot using an adaptive neuro-fuzzy system," *IEE Proc. Control Theory Appl.* **152** (4) 411–426 (July 2005).
21. S. Behnke, "Online trajectory Generation for Omnidirectional Biped Walking," *Proceedings of the 2006 IEEE International Conference on Robotics and Automation*, Orlando, Florida (May 2006) pp. 1597–1603.

https://doi.org/10.1017/S0263574710000627 Published online by Cambridge University Press

22. D. Katić and M.Vukobratović, "Survey of Intelligent Control Algorithms For Humanoid Robots," *Proceedings of the 16th IFAC World Congress*, Prague, Czech Republic, Vol. 16 (July 2005), ISBN: 978-0-08-045108-4, Elsevier Science (27 June 2006).
23. K. H. Park, J. Jo and J. H. Kim, "Stabilization of a Biped Robot Based on Two Mode Q-learning," *2nd International Conference on Autonomous Robots and Agents*, Palmerston North, New Zealand (Dec. 13–15, 2004) pp. 446–451.
24. V. Vapnik, *The Nature of Statistical Learning Theory* (Springer, New York, 1998).
25. J. P. Ferreira, M. M. Crisóstomo, A. P. Coimbra and B. Ribeiro, "Simulation Control of a Biped Robot with Support Vector Regression," *2007 IEEE International Symposium on Intelligent Signal Processing—(WISP'07)*, Madrid, Espanha (Out. 3–5, 2007) pp. 1–6.
26. J. S. R. Jang, "ANFIS: Adaptive-network-based fuzzy inference system," *IEEE Trans. Syst. Man Cybern.* **23**(3), 665–685 (May/June 1993).
27. R. M. Mohamed and A. A. Farag, "Classification of Multispectral Data Using Support Vector Machines Approach for Density Estimation," *IEEE Seventh International Conference on Intelligent Engineering Systems*, *IN*ES03, Assiut, Egypt (March 2003).
28. V. Vapnik, S. Golowich and A. Smola, *Support Vector Method for Multivariate Density Estimation, Advances in Neural Information Processing Systems*, Vol. 12 (MIT Press, April 1999) pp. 659–665.
29. C.-C. Chang and C.-J. Lin, "LIBSVM: A Library for Support Vector Machines," January 2, 2007.
30. J. G. Ziegler and N. B. Nichols, "Optimum settings for automatic controllers", *Trans. ASME* **64**, 759–768 (Nov. 1942).
31. D. M. Katić, A. D. Rodić and M. K. Vukobratović, "Hybrid dynamic control algorithm for humanoid robots based on reinforcement learning," *J. Intell. Robot. Syst.*, **51**(1), 3–30 (Jan. 2008).
32. Y. Nakamura, T. Mori, M.-A. Sato and S. Ishii, "Reinforcement learning for a biped robot based on a CPG-actor-critic method", *Neural Netw.*, **20**(6), 723–735 (Aug. 2007).
33. J. Morimoto, J. Nakanishi, G. Endo, G. Cheng, C. G. Atkeson and G. Zeglin, "Poincaré-Map-Based Reinforcement Learning For Biped Walking," *Proceedings of the 2005 IEEE International Conference on Robotics and Automation (ICRA '05)* (Apr. 18–22, 2005) pp. 2381–2386.
34. K. Hitomi, T. Shibata, Y. Nakamura and S. Ishii, "Reinforcement learning for quasi-passive dynamic walking of an unstable biped robot," *Robot. Autonom. Syst.*, **54**(12), 982–988 (Dec. 31 2006).
35. E. Schuitema, D. G. E. Hobbelen, P. P. Jonker, M. Wisse and J. G. D. Karssen, "Using a Controller Based on Reinforcement Learning for a Passive Dynamic Walking Robot," *5th IEEE-RAS International Conference on Humanoid Robots* (Dec. 5, 2005) pp. 232–237.
36. S. Hyon e G. Cheng, "Disturbance Rejection for Biped Humanoids," *IEEE International Conference on Robotics and Automation*, Roma, Italy (Apr. 10–14, 2007) pp. 2668–2675.
37. S. Kajita, T. Nagasaki, K. Kaneko and H. Hirukawa, "ZMP-based biped running control," *IEEE Robot. Autom. Magaz.* (Disturbance Rejection for Biped Humanoids) **14**(2), 63–72 (June 2007).
38. O. Stasse, A. Escande, N. Mansard, S. Miossec, P. Evrard and A. Kheddar "Real-Time (Self)-Collision Avoidance Task on a HRP-2 Humanoid Robot," *IEEE International Conference on Robotics and Automation*, Pasadena, CA, USA (May 19–23, 2008) pp. 3200–3205.
39. M. R. Heinen and F. S. Osório, "Gait Control Generation for Physically Based Simulated Robots Using Genetic Algorithms", *Lecture Notes in Computer Science* (Advances in Artificial Intelligence), Springer-Verlag, Berlin, Heidelberg (Oct. 2006) pp. 562–571.
40. G. Dip, V. Prahlad and P. D. Kien, "Genetic algorithm-based optimal bipedal walking gait synthesis considering tradeoff between stability margin and speed," *Robotica* (Cambridge University Press, 2008) pp. 1–11.
41. S. J. Yoo, J. B. Park and Y. H. Choi, "Robust control of planar biped robots in single support phase using intelligent adaptive backstepping technique," *Int. J. Control Autom. Syst.* **5**(3), 269–282 (2007).
42. S. H. Lee, J. B. Park and Y. H. Choi, "Sliding Mode Control Based on Self-Recurrent Wavelet Neural Network for Five-link Biped Robot," *SICE-ICASE International Joint Conference*, Busan (Oct. 18–21, 2006) pp. 726–731.
43. J. Or and A. Takanishi, "A Biologically Inspired CPG-ZMP Control System for the Real-time Balance of a Single-Legged Belly Dancing Robot," *Proceedings of IEEE/RSJ International Conference on Intelligent Robots and Systems*, Sendai, Japan (Sep. 28–Oct. 2,, 2004) pp. 931–936.
44. J. P. Ferreira, M. Crisóstomo and A. P. Coimbra, "Rejection of an External Force in the Sagittal Plane Applied on a Biped Robot using a Neuro-Fuzzy Controller," *IEEE International Conference on Advanced Robotics –(ICAR 2009)*, Munich, Germany (June 22–26, 2009) pp. 1–6.
45. J. P. Ferreira, M. Crisóstomo and A. P. Coimbra, "Human gait acquisition and characterization," *IEEE Trans. Instrum. Meas.* **58**(9), 2979–2988 (Sep. 2009).

https://doi.org/10.1017/S0263574710000627 Published online by Cambridge University Press

Appendix

Walking snapshots

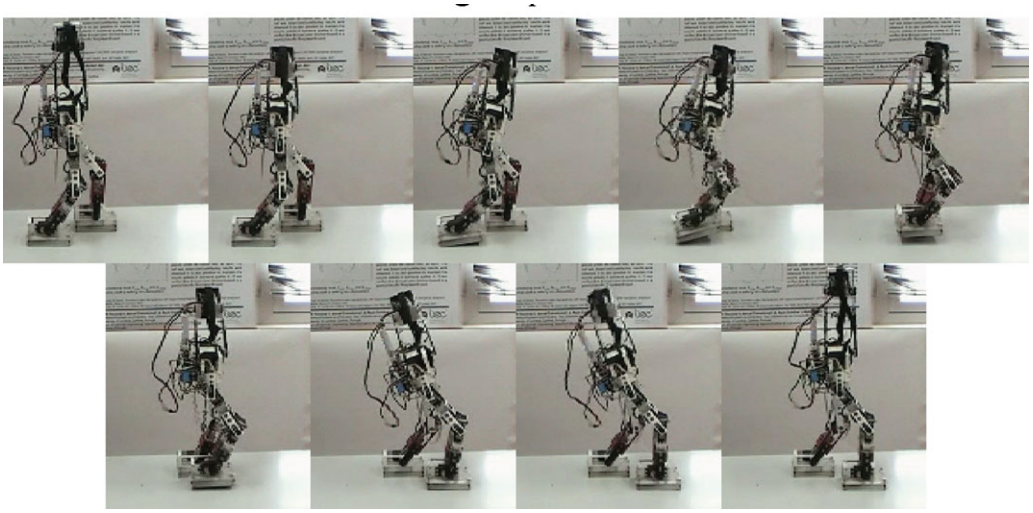

Snapshots of walking on a 10° inclination slope

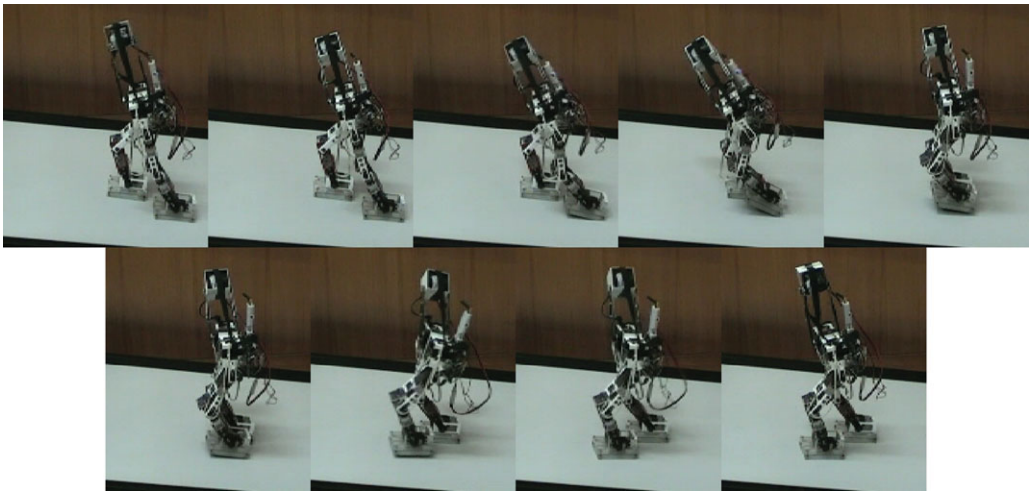

Snapshots of walking on a −10° inclination slope

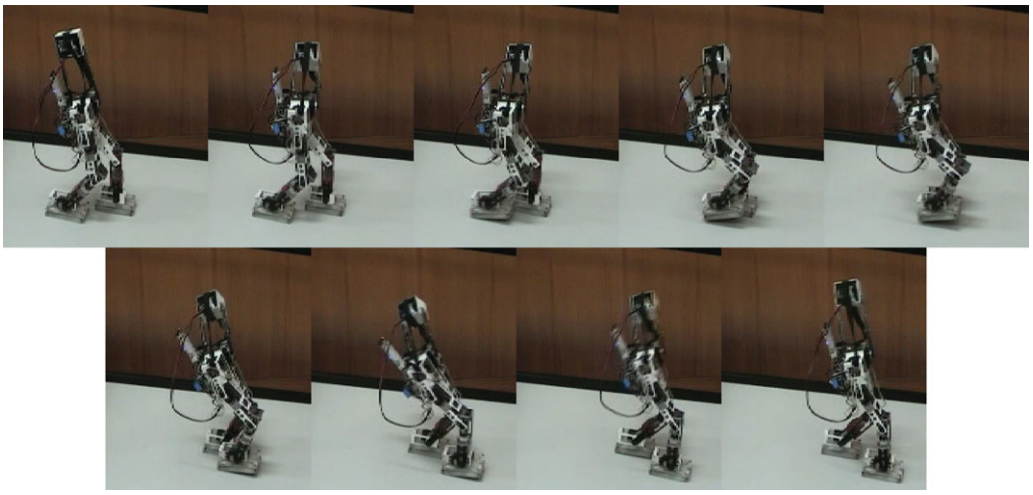

https://doi.org/10.1017/S0263574710000627 Published online by Cambridge University Press